Available online at www.sciencedirect.com
SCIENCE DIRECT®
Tectonophysics 372 (2003) 167–177
TECTONOPHYSICS
www.elsevier.com/locate/tecto

Microearthquakes and faulting in the southern Okinawa Trough

Mamoru Nakamura[a,*], Hiroshi Katao[b]

[a] Department of Physics and Earth Science, Faculty of Science, University of the Ryukyus, Senbaru 1, Nishihara, Okinawa 903-0213, Japan
[b] Research Center for Earthquake Prediction, Disaster Prevention Research Institute, Kyoto University, Uji, Kyoto, Japan

Received 25 June 2002; accepted 1 July 2003

Abstract

Southern Okinawa Trough represents an early stage of back-arc rifting and is characterized by normal faulting and microearthquakes. Earthquake distribution and deep structure of fault was investigated to clarify active rifting in the southern Okinawa Trough, where two parallel grabens are located. A network of ocean bottom seismometers (OBSs) that displayed the hypocenters of 105 earthquakes were observed for a period of 4 days in southern-graben (SG). Most of the microearthquakes occurred in a cluster about 7 km wide, which on a cross-section striking N45°E dips 48° to the southwest. Relocated hypocenters, which are recorded by a local seismic network, show scattered distribution around the southern-graben. There are no remarkable surface faults in the southern-graben. On the other hand, the recalculation of hypocenter locations of 1996 earthquakes swarm recorded by a local seismic network suggests that the swarm is associated with normal faulting on the southern side of northern-graben (NG). Thus, the undeveloped southern-graben is located to the south of the developed northern-graben. Southward migration of rifting, which may be caused by migration of volcanism, could thus be occurring in the southern Okinawa Trough. The extension rate computed for the southern Okinawa Trough from the fault model of the northern-graben is 4.6 cm/year, which is 59–102% of the extension rate (GPS measurements). This result indicates that the majority of extensional deformation is concentrated within the center of the northern-graben in the Okinawa Trough.

Keywords: Back-arc rifting; Okinawa Trough; Extension rate; Earthquake swarm; Seismicity; Fault

1. Introduction

The Okinawa Trough is an active back-arc basin located to the northwest of the Ryukyu Trench and Ryukyu arc (Fig. 1). Geologic and geophysical studies have revealed that the Okinawa Trough is in an early stage of the back-arc rifting (Letouzey and Kimura, 1985; Sibuet et al., 1987, 1998; Park et al., 1998). Temporary GPS sites in the Ryukyu arc have shown movement southward (Imanishi et al., 1996). The direction of present-day extension, estimated from the focal mechanism solution for earthquakes occurring in the axis of the Okinawa Trough, is N175°W (mean azimuth) in the southwestern Okinawa Trough (Fournier et al., 2001).

Recently, analyses based on global positioning system (GPS) measurements have allowed the extension rate between the southern Ryukyu arc and Eurasian plate to be observed directly. GPS measurements by the Geographical Survey Institute of Japan in the southern Ryukyu arc between 1996 and 2001 revealed

* Corresponding author. Fax: +81-98-895-8552.
E-mail address: mnaka@sci.u-ryukyu.ac.jp (M. Nakamura).

0040-1951/$ - see front matter © 2003 Elsevier B.V. All rights reserved.
doi:10.1016/S0040-1951(03)00277-4

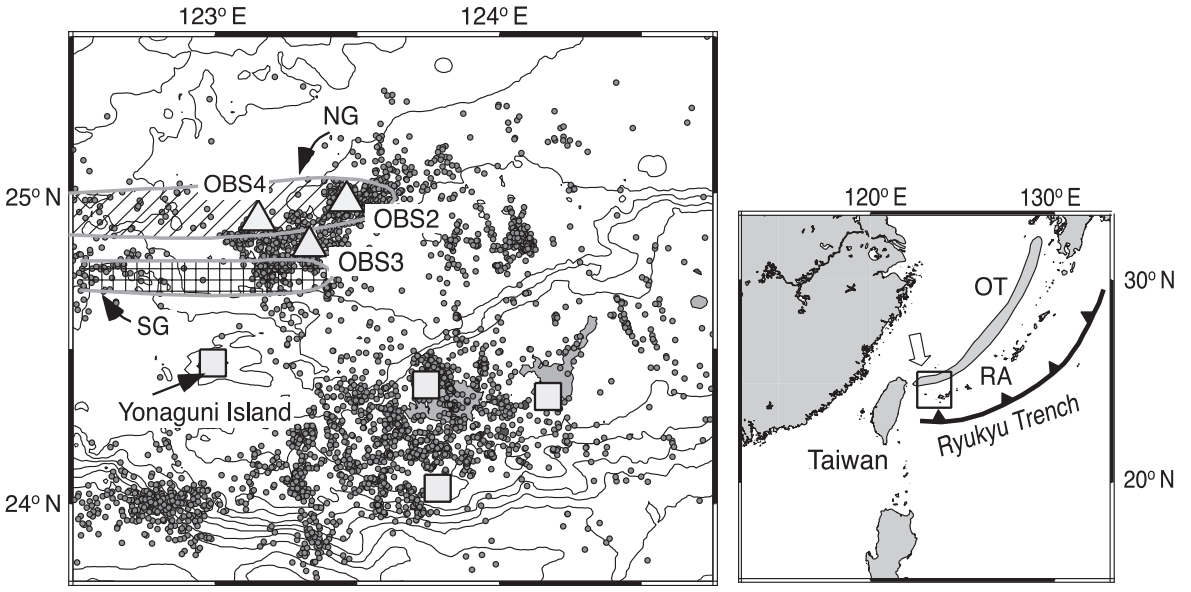

Fig. 1. Bathymetric map of the southern Okinawa Trough region and shallow seismicity between January 1996 and December 1999 (focal depth < 30 km). Bathymetric contour interval is 500 m. Triangles show the locations of the four ocean bottom seismometers. Squares denote the JMA seismic stations used in the relocations. Hatched areas represent northern Graben (Yonaguni Graben; NG) and southern Graben (SG), respectively. OT: Okinawa Trough; RA: Ryukyu arc.

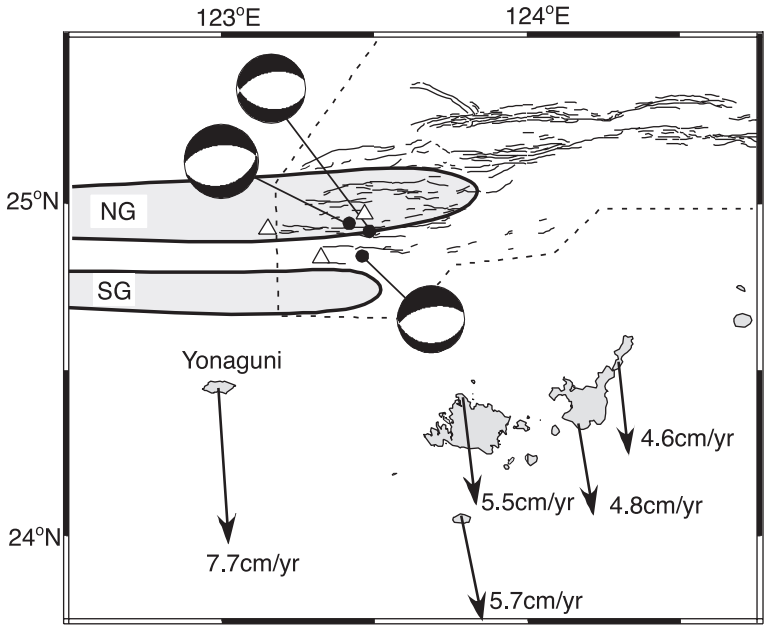

Fig. 2. Fault traces and horizontal displacements in the southern Okinawa Trough. Solid lines are fault traces based on the Seabeam bathymetric map. Dashed line is the limit of the bathymetric map. The horizontal displacements, measured by GPS, of the south Ryukyu arc with respect to south China (Shanghai VLBI station) are shown by solid arrows. CMT solutions for the M5 earthquakes in 1996 are shown on equal-area projections of the lower hemisphere. Hatched areas represent NG and SG, respectively.

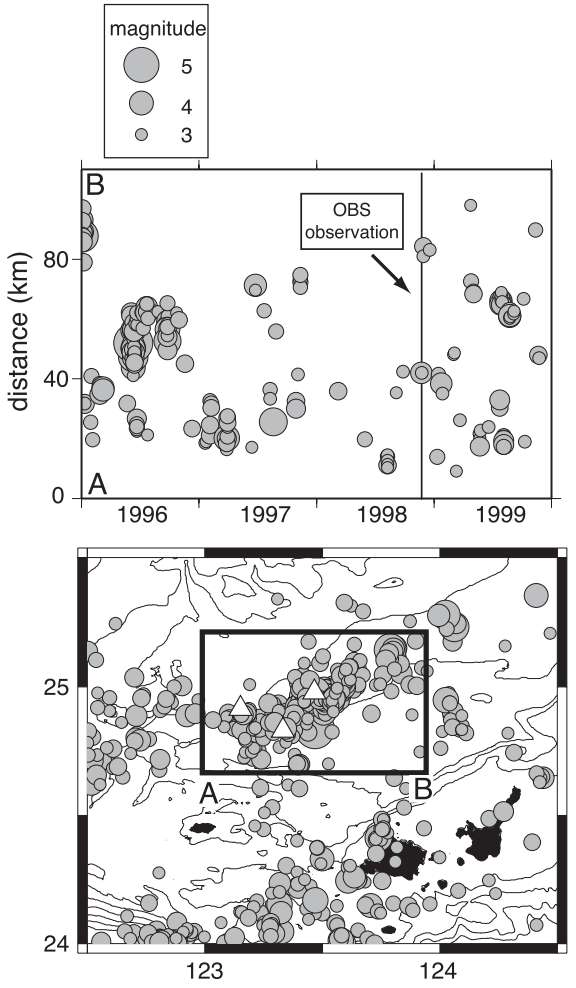

Fig. 3. Space–time distribution of earthquakes ($M \geq 3.0$) along the northern and southern grabens between January 1996 and December 1999.

that the Ryukyu arc is migrating southward (N172°E) with respect to the Shanghai VLBI station in South China (Heki, 1996) (Fig. 2). The extension rate is 4.6 to 5.7 cm/year in the southern Ryukyu arc, except at Yonaguni Island located at the southwestern end of the Ryukyu arc, south of our survey area, where the extension rate is 7.7 cm/year. Back-arc extension is progressing very actively to the north of Yonaguni Island. The extension in the southern Okinawa Trough is perpendicular to the N80°E-trending normal faults (Fig. 2) that form the Graben characteristic of this area.

From topography and seismicity, there are two obvious parallel grabens trending E–W in the southwestern Okinawa Trough (Wang et al., 2000). Northern-graben (NG) is situated between 24°51′N and 24°54′N, and southern-graben (SG) between 24°42′N and 24°48′N (Fig. 1).

The E–W trending normal fault is developed in the NG. The NG extends from 122°50′E to 123°30′E and is seismically very active. The Japan Meteorological Agency (JMA) deployed a telemetered seismic network in the southwest of the Ryukyu arc, which recorded 289 microearthquakes (magnitude $M \geq 3.0$) between January 1996 and December 1999 (Fig. 3). Although swarms of microearthquakes are common in the NG, mainshock–aftershock sequences are rare. In 1996, a major earthquake swarm containing two M5.6 earthquakes was recorded in the NG (Fig. 3). The moment tensor solutions of their events indicated that the movement occurred along a normal fault striking N90°E (Dziewonski et al., 1981) (Fig. 2).

On the other hand, the SG is not as well developed as the NG (Sibuet et al., 1998; Wang et al., 2000). The

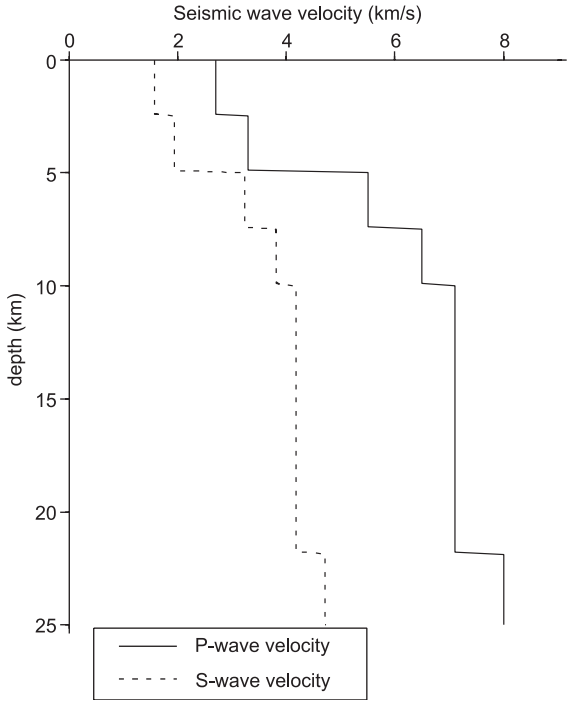

Fig. 4. One-dimensional seismic wave velocity–depth model used for hypocentral determinations. Solid and broken lines show the P and S wave velocity structures, respectively.

SG can only be clearly seen in the east of 122°48′E. To the west of 122°48′E, the shape of the SG disappears.

The seafloor of the area was mapped by Seabeam bathymetry as part of a geophysical survey in the southern Okinawa Trough in July 2000. The geophysical survey also revealed that there are a number of active faults in this area (Fig. 2).

The combination of bathymetry, ocean bottom seismometer (OBS) records, and hypocenters located by local seismic stations forms a detailed seismotectonic picture of the southern Okinawa Trough. In the present report, a detailed seismotectonic analysis of the southern Okinawa Trough is presented based on a comparison of hypocenters obtained using OBS plus the local network, with a fault model obtained by bathymetry.

2. Ocean bottom seismometer network

2.1. Survey site

We deployed four pop-up OBSs in the southern Okinawa Trough between November 19, 1998 and November 23, 1998 with the aid of the *T/S Nagasaki-Maru* of the Faculty of Fisheries, Nagasaki University, Japan. The OBSs were arrayed so as to monitor a 40 × 30 km area, 24°48′–25°12′N and 123°12′–123°36′E, containing the NG axis (Fig. 1). All OBSs were model-IV types made by Kyoto University (Obana et al., 1994), containing velocity-type seismometers with a vertical and two horizontal components, a natural frequency 2 Hz, and a digital recording system. The OBSs recorded continuously and stored the data to magneto-optical disk. OBS-1 did not record any data due to technical problems.

2.2. Methods

A grid search method was employed to accurately locate microearthquakes (Rowlett and Forsyth, 1984; Shen et al., 1997). This method is based on the calculation of the root mean square (rms) travel time residual at regularly spaced, three-dimensional grid points for each earthquake. The horizontal and vertical spacing in this case was 100 m. Arrival times of P and S waves are used for the hypocenter determination.

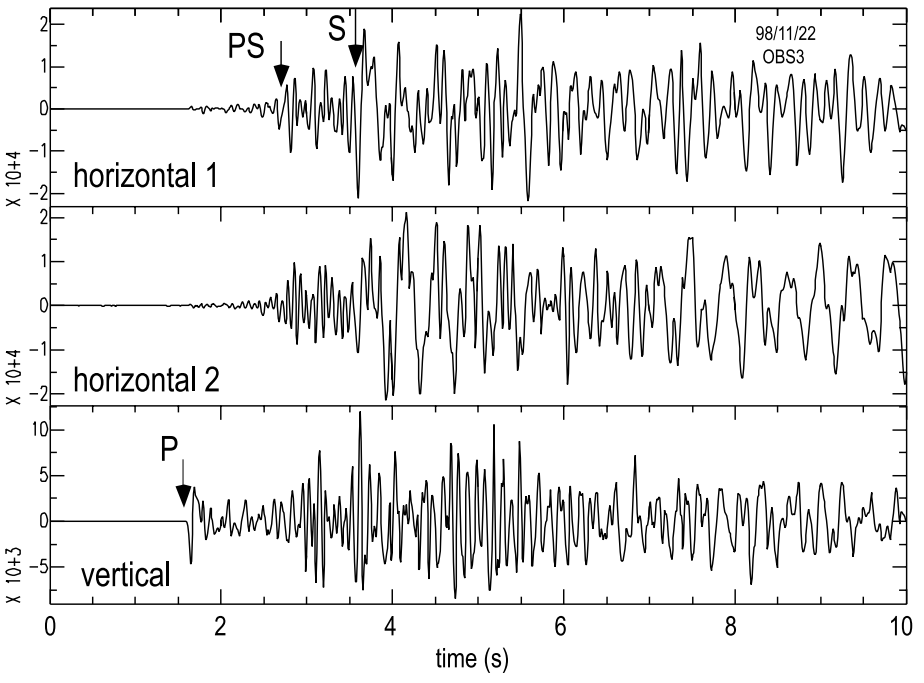

Fig. 5. An example of the microearthquakes, as recorded on the vertical and horizontal seismograms, showing clear P and S arrivals. The converted phase (P-to-S conversion) at the base of the sediment is also observed.

Data weights for P and S phases are 1 and 0.2, respectively. Origin times of the events are estimated using P arrival time vs. S−P time diagram.

The P-wave velocity (V_p) structure of the southern Okinawa Trough obtained through seismic refraction studies (Hirata et al., 1991) was employed for reference (Fig. 4). Although the depth of the Moho varies from 18 to 25 km in the southern Okinawa Trough (Sibuet et al., 1995), an average depth of 22 km was employed in this study.

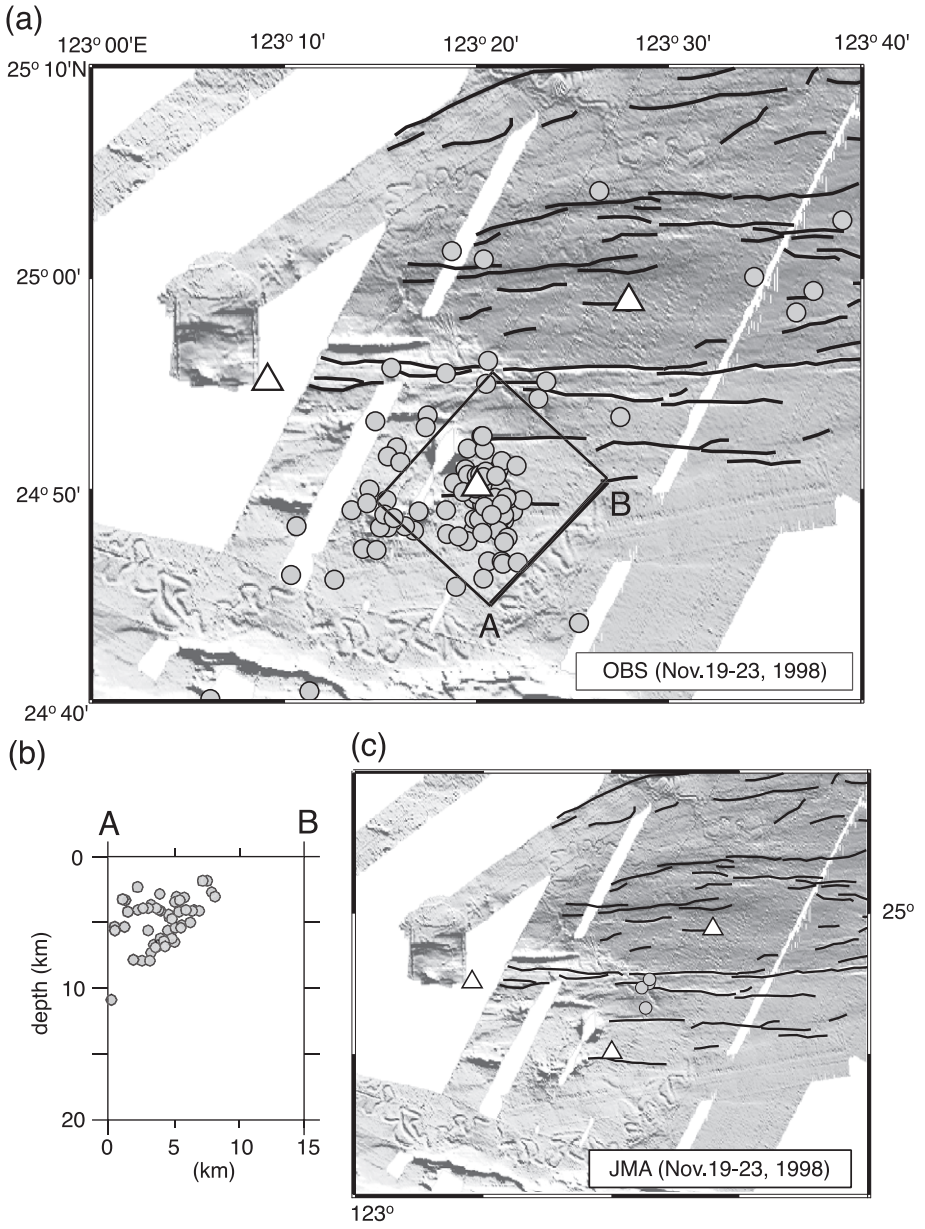

Fig. 6. Distribution of the 105 microearthquakes recorded during the 4-day deployment. (a) Epicenter locations (circles). Triangles indicate the location of OBSs. (b) Projection of the hypocenters on the vertical plane in the N45°E direction. The depths of the microearthquakes range from 2 to 10 km. (c) Epicenter locations (circles) recorded by JMA network.

This model was adopted for all analyses except for that of the surface sedimentary layer, because the thickness of sedimentary layer changes greatly from place to place. We estimated the thickness of this layer at each station from the interval between the P-phase and P to S conversion from the P wave to the S wave at the boundary between the sedimentary layer and the crustal layer (PS) (Fig. 5). For the sediment, we assumed a V_p of 2.0 km/s and V_p/V_s ratio of 2.76 on the basis of previous OBS observations (Nagumo et al., 1986; Iwasaki et al., 1990; Hirata et al., 1991). The intervals between P and PS arrivals at OBS-2, OBS-3, and OBS-4 were 0.70, 1.0, and 1.2 s, respectively, implying computed sedimentary thicknesses of 0.80, 1.2, and 1.4 km, respectively. We incorporated the effect of the sedimentary layer into the station correction for each station. Station corrections 0.40, 0.60, and 0.70 s for the P-phase, and 1.10, 1.66, and 1.93 s for the S-phase were applied at OBS-2, OBS-3, and OBS-4, respectively. The V_p/V_s ratio of the crustal layer was assumed to be 1.73.

2.3. Hypocenter locations

A total of 105 local events were observed (Fig. 6a). Four events were recorded by both land-based JMA network and the OBSs network (Fig. 6c). Most of the microearthquakes occurred in a cluster about 7 km wide in the 24°50′N 123°20′E area, which corresponds to the SG (Fig. 6). Magnitudes of the events range between 1.0 and 4.3. The east–west, north–south, and vertical uncertainty in location are within 0.5, 1.0, and 1.0 km, respectively. Focal depths range from 2 to 12 km. A projection of the hypocenters onto a vertical cross-section striking N45°E shows that the cluster of microearthquakes falls on a plane dipping 48° to the southwest.

A composite of the polarities of clear P arrivals from the southwest dipping microearthquake cluster was produced, and a focal mechanism solution was estimated. We computed the composite focal plane using the events in the dipping plane. The best-fitting fault plane solutions for the composite polarities were normal faults striking N139°E or N201°E. The nodal plane of the N139°E fault dips 65° southwestward (Fig. 7). This fault has a strike similar to the microearthquakes plane (Fig. 6). The cluster of seismicity is then associated with the same fault plane. Strike of the estimated fault is not similar to those of faults in the NG, showing that orientation of faults may be disarranged in the SG.

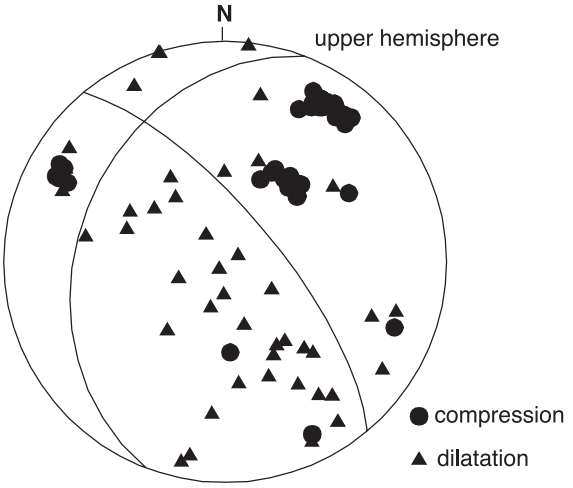

Fig. 7. Focal mechanism solution with composite polarities of P arrivals from 42 microearthquakes. The polarities and focal mechanism solution are plotted in the upper focal sphere. Circles are compressional arrivals, and triangles are dilatational arrivals.

The seismic plane is not oriented parallel to the fault of NG, probably related to the influence of the stress field of the edge of the SG near the cluster.

3. Relocation of local seismic network data

3.1. Methods

The JMA has also carried out seismic observations in the Ryukyu arc. However, the locations of hypocenter were not sufficiently accurate for our purposes because the seismic stations were established only on land. In order to compare the seismicity with the fault distribution in the NG, we recomputed the locations of earthquakes recorded between 1996 and 1999 using a local seismic network. Since epicentral distances are less than 100 km, Pn phases are not observed. Therefore lateral variation of depth of Moho discontinuity does not affect the hypocenter determination in this study. Station corrections were obtained by relocating events based on recordings of the same events by our OBS network, using the corrected P and S arrivals times for relocation. The grid-search method

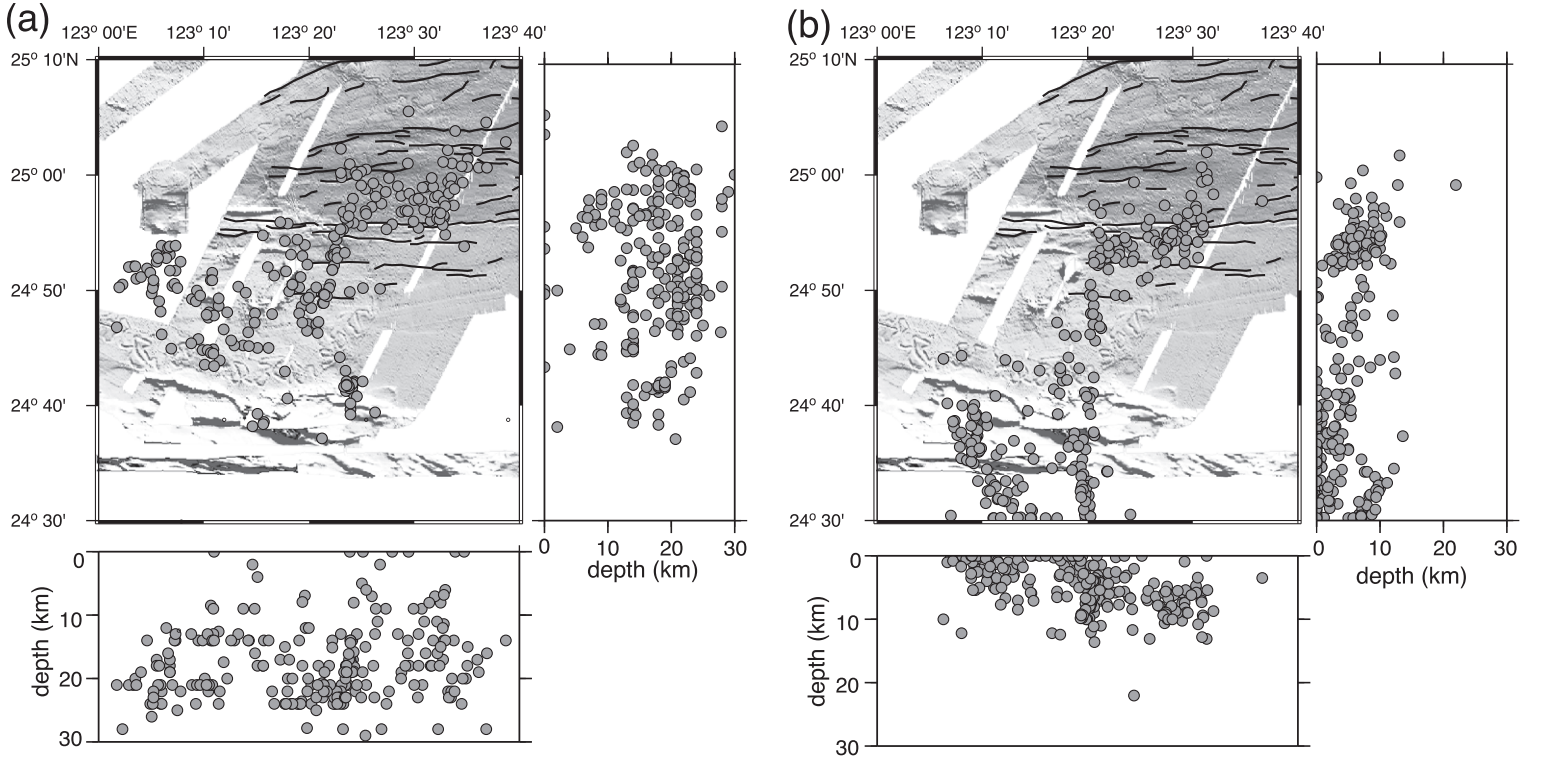

Fig. 8. Distribution of 241 microearthquakes recorded by JMA over 4 years. Circles indicate the events. (a) Initial epicenter locations before relocation. (b) Final epicenter locations after relocation.

as used for analyzing the OBS data was employed for relocation of the JMA hypocenters. A total of 241 earthquakes were relocated.

3.2. Hypocenter locations

The relocated hypocenters are distributed to the south of the JMA hypocenters (Fig. 8). The depths of the hypocenters changed from 20–40 to 0–10 km. The east–west, north–south, and vertical uncertainties are E–W 5 km, N–S 12 km, and 12 km, respectively.

Relocated hypocenters show scattered distribution in the SG. On the other hand, these are clustered and aligned to E–W direction in the NG. Then we estimated error of relative location caused by velocity uncertainty to verify difference of hypocenter distribution. We assigned positive velocity anomaly with magnitude of 5% to the 1-D velocity structure and relocated hypocenters. The result shows that the error of relative location is within 3 km, which is smaller than the hypocentral error. Thus the scattered distribution of hypocenters in the SG and the E–W trending distribution in the NG are not generated by the hypocenter determination.

Most of the earthquakes occurred in a band about 11 km wide and 20 km long parallel to the south of the E–W trending faults of NG in the east of 123°20′E. The lower limit for the seismogenic depth is 10 km. The events examined are part of an earthquake swarm in 1996, the epicenters of which define a lineament trending N90°E. This is parallel with the strike of the normal fault plane of the M5 events and the fault trend (Fig. 2), suggesting that the 1996 swarm was associated with the normal faults that passed through the south of the NG.

The relocated microearthquakes occurred around the SG in the west of 123°20′E. The epicenters are located 20 km to the south of the JMA epicenters (Fig. 8). Most of the events are part of earthquake swarms. The earthquakes are scattered in a north–south direction because the uncertainty in the north–south direction is large. However, the hypocenters are observed to be concentrated in a topographically undulating area. Surface faults were not found. However, a knoll, elongated east-to-west, fills this area, with a small graben to the west (Sibuet et al., 1998). The normal faulting that forms the knoll and the small graben suggest to be the origin of these earthquake swarms.

The distribution of hypocenters and surface faults should show a difference in the development of the two grabens. E–W striking faults dominate in the NG. The 1996 swarm clustered along an E–W direction trend of 20 km in length in the southern faults of the NG. This suggests that the 1996 swarm in the NG occurred in the developed faults. Hypocenters are scattered in the SG. However, the fault plane of the 1998 swarm is oblique to that of the NG. Noticeable surface faults are not found in the SG. This suggests that the rifting is undeveloped in the SG.

Analysis of seismicity shows that the undeveloped graben is located to the south of the developed NG. Graben development thus migrated southward in the southwestern Okinawa Trough (Sibuet et al., 1998). We propose that migration of volcanism causes the migration of graben development in the southwestern Okinawa Trough. A volcanic chain of seamounts, cutting across obliquely on the southwestern Okinawa Trough, occurs along a 70-km-long NE oriented zone (Sibuet et al., 1998). This cause of the volcanism could lie in the partial melting of the subducted oceanic ridge and the oblique subduction of Philippine Sea plate (Sibuet et al., 1998). The southwestern end of the volcanic chain is located in the SG. Elastic lithosphere would be thinned locally by the volcanism, and consequently, rifting may migrate southward.

4. Fault system and extension rate of the NG

We have constructed a possible fault model for the NG in order to estimate the extension rate of the southern Okinawa Trough. The north–south bathymetric profile, which crosses the NG, shows that the NG is asymmetric (Fig. 9), having a much steeper southern slope. The 1996 swarm occurred in the southern part of the NG, and epicenters of the swarm exhibit a clear east–west trend. These results are consistent with the simple hypothesis that a single large listric normal fault undercuts the NG. Asymmetric half-graben structures formed by listric faulting are common in the southern Okinawa Trough (Park et al., 1998).

We divided the listric fault into flat and ramp faults as shown in Fig. 8b and computed the dip and slip of both faults. Surface deformation due to the fault slip

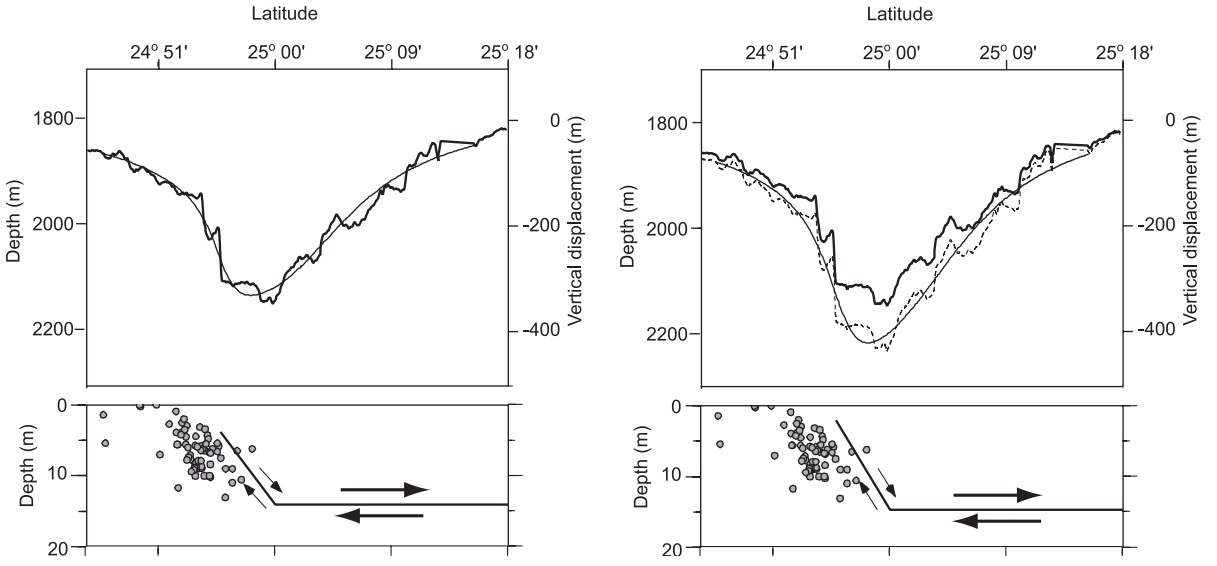

Fig. 9. (Top) Vertical displacement (solid lines) deduced from the dislocation model and basement topography (bold lines). Dashed line shows the basement after sediment layer correction. Top-left and top-right show the bathymetry model and sediment-stripped model, respectively. (Bottom) Fault model. Parameters for this model are listed in Table 1. Circles indicate earthquake hypocenters.

was calculated based on dislocation theory in an elastic half space (Okada, 1985). The fault parameters were determined by matching vertical dislocation profile to bathymetry data (bathymetry model). The shear modulus was set to 3×10^{10} Pa. The origin of the profile is 25°15′N, and cuts north–south.

Fig. 9 and Table 1 described the best-fit bathymetry model. The ramp fault dips 53° to the north from a depth of 3.8 to 14 km. This corresponds to the nodal plane of the Centroid Moment Tensor solution for the 1996 swarm (Fig. 2). The flat of the fault lies horizontally at a depth of 14 km, corresponding to the lower limit of the observed seismicity. The dip–slip of the ramp and flat faults are 210 and 920 m, respectively.

Table 1
Dislocation model

Model	Subfault[a]	Width (km)	Dip (deg.)	Displacement (m)	Depth of fault upper edge (km)
Bathymetry	1	13.2	54	210	3.8
	2	>50.0	0	920	14.1
Sediment-stripped	1	12.1	53	334	2.0
	2	>50.0	0	1115	14.6

[a] Subfaults were computed with a fixed strike of N90°E.

We then estimated the fault model by stripping the sediment after the initiation of the NG. The seismic reflection survey showed that thickness of sediment layer since late Pleistocene in the Graben is twice as large as that outside of the Graben in the south Okinawa Trough (Fig. 10). The extinct submarine channels, which are cut by the NG, have been covered by thin (a few tens of meters) sediments (Sibuet et al., 1998). Assuming that the sedimentation above the channels started after the initiation of the NG, thickness of the sediment layer in the NG is estimated within 100 m. Then the faults model (sediment-stripped model) was computed by matching vertical dislocation profile to bathymetry data stripping the sediment layer. The dip–slip of the ramp and flat faults are 334 and 1115 m, respectively (Table 1, Fig. 9). Thus, stripping the sediment layer induces the increase in dip–slip of the fault, although location of the faults is slightly changed.

The slip velocity of the fault was then computed. The initiation of faulting was estimated based on the age of several extinct submarine channels with numerous meanders in the southern Okinawa Trough. The extinct submarine channels are as young as 20,000 years old (Sibuet et al., 1998), and, as these

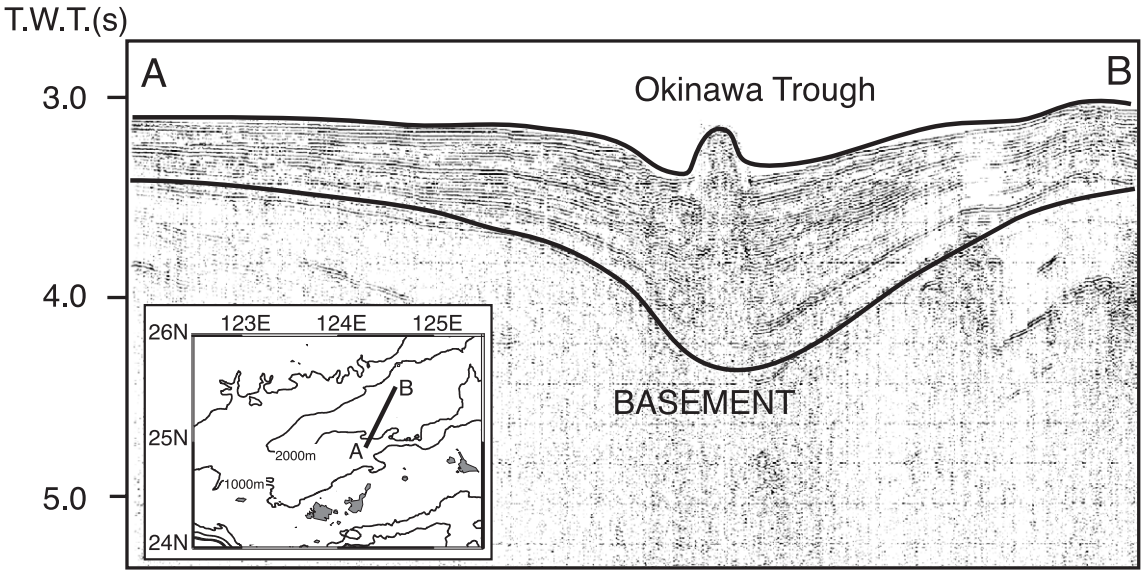

Fig. 10. Single-channel seismic reflection profile and its interpretation showing the south Okinawa Trough. Location of this section is shown as thick line in the location map.

channels are offset several times by the E–W trending normal faults, the initiation of faulting is considered to be more recent than 20,000 years ago (Sibuet et al., 1998). Those ages of 20,000 years was then assumed for the initiation of faulting. If the slip rates of the faults were constant, the dip–slip rates on ramp and flat faults are 1.1–1.7 and 4.6–5.6 cm/year, respectively. The observed extension rate in the southern Okinawa Trough as measured by GPS is 5.5–7.7 cm/year (Fig. 2). On the other hand, the geological extension rate as estimated by migration of volcanism is 3 cm/year (Sibuet et al., 1998). Therefore, the dip–slip rate of the flat fault is 59–102% (GPS) or 153–187% (geological) of the extension rate. Large contribution over 100% as estimated using geological data might be caused by the uncertainty of initiation age of normal faults. However, the deep flat faulting is expected to contribute to extension and deformation in the Okinawa Trough, and suggests that the majority of the extensional deformation occurs in the center of the rifting region of the Okinawa Trough.

The displacement on the ramp fault is one-third of that on the flat fault. The smaller displacement on the ramp fault is considered to be due to fault branching. Listric normal faults generally branch into antithetic faults near the surface in half-graben areas (White et al., 1986). Therefore, the dip–slip of the flat fault would be divided between the ramp fault and the antithetic faults (Villamor and Berryman, 2001). In the case of the NG, the cumulative dip–slip near the surface, obtained by summing the vertical component of displacement on small faults in the Graben, is 700 m. This is similar to the dip–slip on the flat fault, indicating that the difference between the slip rate of the ramp fault and the flat fault is due to branching of the listric normal fault near the surface.

5. Conclusions

This study provides new constraints on the development of southwestern Okinawa Trough.

Analysis of seismicity shows the different hypocenters distribution in two parallel grabens of the southwestern Okinawa Trough. NG is well developed, and the swarm in the NG occurred in the developed faults. However, hypocenters are scattered in the undeveloped SG. Analysis of seismicity suggests that the undeveloped graben is located in the south of developed NG. SG is located in the southern end of the volcanic chain. We propose a hypothesis that migration of volcanism causes the southward migra-

tion of graben. Elastic lithosphere would be thinned locally by the volcanism, and consequently, rifting extension may occur.

The extension rate computed for the southern Okinawa Trough from the fault model of the NG is 4.6 cm/year, which is 59–102% of the extension rate observed by GPS measurements. This result indicates that the majority of extensional deformation is concentrated within the center of the rifting area in the Okinawa Trough.

Acknowledgements

We thank the captain and crew of the *T/S Nagasaki-Maru* for their help with data collection. We also thank the staff of the Japan Meteorological Agency for providing the preliminary JMA hypocenter data, and the captain and crew of the *R/V Yokosuka*. We appreciate the valuable comments made by anonymous reviewers, which helped us greatly to improve the manuscript. Generic Mapping Tools software was used to display some of the figures (Wessel and Smith, 1991). This research was supported by the Disaster Prevention Research Institute, Kyoto University (grant number IOG-11) and Earthquake Research Institute, University of Tokyo (grant number 2000-B-05).

References

Dziewonski, A.M., Chou, T.A., Woodhouse, J.H., 1981. Determination of earthquake source parameters from waveform data for studies of global and regional seismicity. J. Geophys. Res. 86, 2825–2852.

Fournier, M., Fabbri, O., Angelier, J., Cadet, J.-P., 2001. Regional seismicity and on-land deformation in the Ryukyu arc: implications for the kinematics of opening of the Okinawa Trough. J. Geophys. Res. 106, 13751–13768.

Heki, K., 1996. Horizontal and vertical crustal movements from three-dimensional vary long baseline interferometry kinematic reference frame: implications for the reversal time scale revision. J. Geophys. Res. 101, 3187–3198.

Hirata, N., Kinoshita, H., Katao, H., Baba, H., Kaiho, Y., Koresawa, S., Ono, Y., Hayashi, K., 1991. Report on DELP 1988 cruises in the Okinawa Trough: Part 3. Crustal structure of the southern Okinawa Trough. Bull. Earthq. Res. Inst. Univ. Tokyo 66, 37–70.

Imanishi, M., Kimata, F., Inamori, N., Miyajima, R., Okuda, T., Takai, M., Hirahara, K., 1996. Horizontal displacements by GPS measurements at the Okinawa–Sakishima islands (1994–1995). Zisin 2 (49), 417–421 (in Japanese).

Iwasaki, T., Hirata, N., Kanazawa, T., Melles, J., Suyehiro, K., Urabe, T., Moller, L., Markis, J., Shimamura, H., 1990. Crustal and upper mantle structure in the Ryukyu island arc deduced from deep seismic sounding. Geophys. J. Int. 102, 631–651.

Letouzey, J., Kimura, M., 1985. Okinawa Trough genesis: structure and evolution of a back-arc basin developed in a continent. Mar. Pet. Geol. 2, 11–130.

Nagumo, S., Kinoshita, H., Kasahara, J., Ouchi, T., Tokuyama, H., Asanuma, T., Koresawa, S., Akiyoshi, H., 1986. Report on DELP 1984 cruises in the middle Okinawa Trough: Part II. Seismic structural studies. Bull. Earthq. Res. Inst. Univ. Tokyo 61, 167–202.

Obana, K., Katao, H., Matsuo, S., Ando, M., 1994. Development of a new ocean bottom seismometer (Model IV of Kyoto University). Bull. Disaster Prev. Res. Inst. Kyoto Univ. 44, 199–210.

Okada, Y., 1985. Surface deformation to shear and tensile faults in a half-space. Bull. Seismol. Soc. Am. 75, 1135–1154.

Park, J.O., Tokuyama, H., Shinohara, M., Suyehiro, K., Taira, A., 1998. Seismic record of tectonic evolution and backarc rifting in the southern Ryukyu island arc system. Tectonophysics 294, 21–42.

Rowlett, H., Forsyth, D.W., 1984. Recent faulting and microearthquakes at the intersection of the Vema Fracture zone and the Mid-Atlantic ridge. J. Geophys. Res. 89, 6079–6094.

Shen, Y., Forsyth, D.W., Conder, J., Dorman, L.M., 1997. Investigation of microearthquake activity following an intraplate teleseismic swarm on the west flank of the Southern East Pacific Rise. J. Geophys. Res. 102, 459–475.

Sibuet, J.C., Letouzey, J., Barbier, F., Charvet, J., Foucher, J.P., Hilde, T.W.C., Kimura, M., Chiao, L.Y., Marsset, B., Muller, C., Stephan, J.F., 1987. Backarc extension in the Okinawa Trough. J. Geophys. Res. 92, 14041–14063.

Sibuet, J.-C., Hsu, S.-K., Shyu, C.-T., Liu, C.-S., 1995. Structural and kinematic evolutions of the Okinawa Trough backarc basin. Backarc Basins: Tectonics and Magmatism, 343–379.

Sibuet, J.C., Deffontaines, B., Hsu, S.K., Thareau, N., Le Formal, J.P., Liu, C.S., ACT party, 1998. Okinawa trough backarc basin: early tectonic and magmatic evolution. J. Geophys. Res. 103, 30245–30267.

Villamor, P., Berryman, K., 2001. A late Quaternary extension rate in the Taupo Volcanic zone, New Zealand, derived from fault slip data. N.Z. J. Geol. Geophys. 44, 243–269.

Wang, C., Yang, M.-L., Chou, C.-P., Chang, Y.-C., Lee, C.-S., 2000. Westward extension of the Okinawa Trough and its western end in the northern Taiwan area: bathymetric and seismological evidence. TAO 11, 459–480.

Wessel, P., Smith, W.H.F., 1991. Free software helps map and display data. EOS Trans. AGU 72, 441.

White, N.J., Jackson, J.A., McKenzie, D.P., 1986. The relationship between the geometry of normal faults and that of the sedimentary layers in their hanging walls. J. Struct. Geol. 8, 897–909.